Supporting Information

A Niobium Oxide with Shear Structure and Planar Defects for High-Power Lithium Ion Batteries

Tongtong Li,[ab#] Gyutae Nam,[a#] Kuanting Liu,[c] Jeng-Han Wang,[c] Bote Zhao,[ag*] Yong Ding,[a] Luke Soule,[a] Maxim Avdeev,[de] Zheyu Luo,[a] Weilin Zhang,[a] Tao Yuan,[a] Panpan Jing,[a] Min Gyu Kim,[f*] Yanyan Song [b*] and Meilin Liu [a*]

[a]School of Materials Science and Engineering, Georgia Institute of Technology, Atlanta, GA 30332-0245, USA

[b]College of Sciences, Northeastern University, Shenyang, 110004, China.

[c]Department of Chemistry, National Taiwan Normal University, 88, Sec. 4 Ting-Zhou Road, Taipei 11677, Taiwan, R.O.C.

[d]Australian Centre for Neutron Scattering, Australian Nuclear Science and Technology Organization, Sydney, Australia

[e]School of Chemistry, The University of Sydney, Sydney 2006, Australia

[f]Beamline Research Division, Pohang Accelerator Laboratory (PAL), Pohang University of Science and Technology (POSTECH), Pohang, Republic of Korea

[g]School of Environment and Energy, South China University of Technology, Guangzhou 510006, China

[#]T.L. and G.N. contributed equally to the work.

*Corresponding author: botezhao@scut.edu.cn; mgkim@postech.ac.kr; yysong@mail.neu.edu.cn; meilin.liu@mse.gatech.edu

Experimental section

Materials Synthesis. The composition of Nb_2O_5 hydrate (CBMM Company) was characterized using energy-dispersive X-ray spectroscopy **(EDS, Figure S2)**. To obtain Nb_2O_5 of desired phases and defects, Nb_2O_5 hydrate powder was calcined in an alumina crucible placed in a box furnace at different temperatures (700, 850, 900, 950, 1000, 1100, or 1300 ^oC) for 3 hours. The furnace exposed to ambient air was heated up at a rate of 5 $^oC\ min^{-1}$ to the calcination temperature. For preparing the H-Nb_2O_5 with same particle size as d-H-Nb_2O_5, the sample obtained at 1300 ^oC was roller milled with zirconium ball in ethanol overnight, and then dried in a drying oven.

Characterization.

Thermal gravimetric analysis (TGA). A Q600 SDT system (from TA Instruments) was used for TGA. To mimic the condition used for the synthesis of the samples, the Nb_2O_5 hydrate powder was placed in an alumina crucible exposed to flowing air (at 20 mL min^{-1}). The sample was heated up at a rate of 5 $^oC\ min^{-1}$ from 25 to 1000 ^oC.

Raman measurements. Raman spectroscopic measurement of Nb_2O_5 powder samples was performed on a Renishaw RM1000 microspectroscopic system with a 50x objective and an Ar laser excitation (633 nm). For the *ex-situ* Raman measurement of lithiated Nb_2O_5 pellet, a green laser with a wavenumber of 514 nm was used to enhance signal strength. Every sample was measured at least three times in different regions and the data averaged. Every spectrum was acquired over a collection time of 60 s with two accumulations.

X-ray Diffraction (XRD). XRD patterns of samples were recorded at room temperature using an X'Pert PRO Alpha-1 X-ray diffractometer with a Cu Kα radiation source. Patterns were recorded from 8−80° 2θ in steps of 0.008° 2θ. The crystal structure was visualized using CrystalMaker® CrystalMaker Software Ltd, Oxford, England (www.crystalmaker.com) and VESTA.[1] The structure refinement of XRD patterns were performed using the FullProf Suite software.

Scanning electron microscopy (SEM) analysis. SEM analysis was performed on a Hitachi SU8010 SEM with a beam voltage of 5 kV. EDS of Nb_2O_5 hydrate was performed using a Zeiss Ultra 60 FE-SEM at an accelerating voltage of 10 kV.

Transmission electron microscopy (TEM) analysis. A high-resolution TEM analysis was carried out using FEI G2 Tecnai F30. JEMS software from Dr. Stadelmann was used to do the HRTEM simulation.[2]

Specific surface area analysis. Surface area were measured by Micromeritics TriStar II Surface and Porosity Analyzer through BET methods.

***Operando* X-ray absorption spectroscopy (XAS).** *Operando* XAS was conducted on the multipole-wiggler BL10C beam line at the Pohang light source (PLS-II) with top-up mode operation under a ring current of 360 mA at 3.0 GeV. Monochromatic X-ray beams were acquired with a liquid nitrogen-cooled double-crystal monochromator (Bruker ASC) with available in situ exchange in vacuum between a Si (111) and Si (311) crystal pair. For Nb K-edge XAS measurements, the Si (111) crystal pair was used. Homemade electrochemical pouch-type half-cells with polyimide film windows were assembled for *operando* XAS measurements on 700 °C Nb_2O_5 and 950 °C Nb_2O_5 samples, in transmittance mode using N_2 gas-filled ionization chambers (IC-SPEC, FMB Oxford) for the incident and transmitted X-ray photons. To remove higher-order harmonic contaminations of incident X-ray intensity (I_0), the beam intensity has been detuned to ~70 % of I_0. Energy calibration processes were conducted for each XAS measurement with reference Nb foil placed in front of the third ion chamber. XAS spectra for Nb were collected with scanning time of 25 minutes for one spectrum under 0.25 C-rate of charge and discharge while 24 seconds for one spectrum under 10 C-rate of charge and discharge. Under 0.25 C-rate of charge and discharge, 30 scans of XAS spectra for both 700 °C Nb_2O_5 and 950 °C Nb_2O_5 samples were conducted to acquire the reliable electronic/crystalline structures. While under 10 C-rate of charge and discharge, 14~16 scans of XAS spectra for Nb_2O_5 samples were collected to obtain the reliable electronic/crystalline structures. Based on the standard XAS analysis procedure, the conversion of spectra data were performed into the normalized XANES and Fourier-transformed radial distribution functions (RDF). AUTOBK and FEFFIT modules in UWXAFS package were used to obtain the k^3-weighted Nb K-edge EXAFS spectra, $k^3\chi(k)$, with the removal of background and the normalization processes on the edge jump. The $k^3\chi(k)$ spectra were Fourier-transformed (FT) in the k range between 1.0 and 12.0 $Å^{-1}$.

Computational methods. The exchange-correlation functional was treated by generalized gradient approximation (GGA) with the Perdew-Wang (PW91) parameterization. The projector-augmented wave method (PAW) was employed to calculate the electron density that core electrons were treated with cost-effective pseudopotentials and valence electrons were expanded by plane-wave basis set with the kinetic cutoff energy at 600 eV. The Brillouin-Zone (BZ) integration was sampled by the Monkhorst-Pack scheme at 0.05 ×2 (1/Å) interval in the reciprocal space. The

structural optimization was performed using the quasi-Newton method with the energy and gradient convergences of 1×10^{-4} and 1×10^{-2} eV, respectively. 3DBVSMAPPER developed to generate bond-valence sum maps was used to depict the lithium diffusion pathway in the crystal structure.[3]

Electrochemical measurements. In a typical electrode preparation, a binder (e.g., PVDF) was first dissolved in 1-methyl-2-pyrrolidone (NMP, Sigma-Aldrich, 99.5%, anhydrous). The anodes slurry were prepared by manual grinding active material (Nb_2O_5) with carbon (SUPER P Li, TIMCAL) and binder in the mass ratio of 8:1:1 in a mortar. Then the slurry was dispensed on a copper foil and doctor-bladed to approximately 20 μm thick to achieve an active material mass loading of 1.0~1.5 mg cm^{-2}. The foil was first dried in a drying oven in air at 80 °C for 30 minutes and then transferred into a vacuum oven and dried at 90 °C overnight. No calendering steps were used in this work. The electrodes were finally punched into disk-shape films (diameter in 10 mm) and transferred to an argon-filled glovebox for assembling. The electrolyte is 1.0 M lithium hexafluorophosphate ($LiPF_6$) in ethylene carbonate/dimethyl carbonate (EC/DMC, 1:1 by volume) solution (Sigma-Aldrich). The glass microfiber (Whatman) was used as separator and metallic Li (MTI) was used as both reference and counter electrode. The half-cells (CR2032 coin type cell) were used for battery tests and dwelled overnight before testing. The electrochemical tests were carried out using 8-channel Neware battery system (CT4008) at room temperature (approximately 22 °C). The charge-discharge cycling was performed at a constant current, which is converted to C-rate based on the theoretical capacity of Nb_2O_5 (~200 mAh g^{-1}). Cyclic voltammetry (CV) measurements were performed at room temperature using an electrochemical workstation (Solartron, SI 1285). The GITT experiments were performed at a current density of C/10 (20 mA g^{-1}), a current pulse width of 0.5 h, and a rest step of 12 h to reach quasi-equilibrium potential. $D_{Li}L^{-2}$ value (instead of D_{Li}) was extracted from the following equation to eliminate the effect of circuitry of the electrode.[4, 5]

$$\tilde{D}_i = \frac{4}{\pi \times \tau} \cdot L^2 \cdot \left(\frac{\Delta E_S}{\Delta E_t}\right)^2$$

where τ is the duration of the current pulse, L is the diffusion length, ΔE_S is the change in steady-state potential, ΔE_t is the total change of the cell voltage during the current pulse after removing the ohmic loss.

For the preparation of lithiated Nb_2O_5 for *ex-situ* Raman and XRD measurements, ~150 mg of

Nb_2O_5 powder was pressed to a 10 mm dense pellet, which was then assembled in a Swagelok cell as the working electrode while keeping the other condition the same as the coin cell. The cell was discharged at 0.1 mA cm^{-2} (≈0.0026 C) to different cutoff voltages and then was disassembled in a glovebox. The pellet was rinsed with DMC to clean electrolyte residues and was dried in the glovebox. For the measurement of *operando* X-ray absorption spectroscopy, we have prepared home-made electrochemical pouch-type half-cells with the same electrode and electrolyte, etc. All pouch-type half-cells were assembled in aluminum laminated film.

The data points in Ragone plot for comparison were extracted from corresponding literature using WebPlotDigitizer.[6]

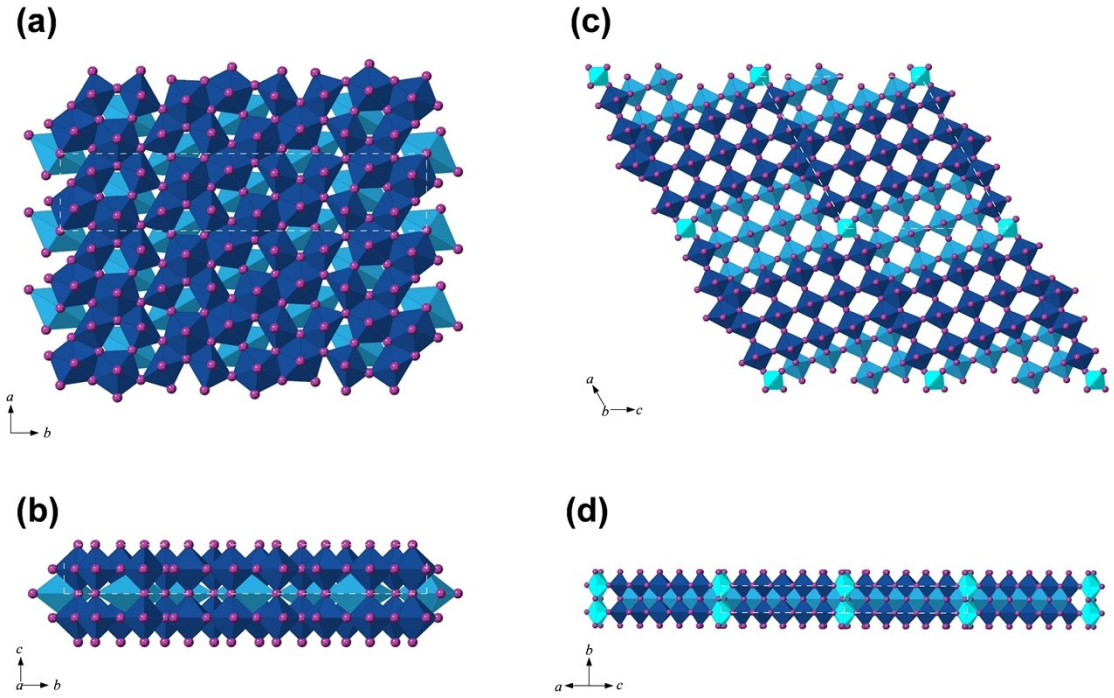

Figure S1. Crystal structure of T-Nb_2O_5 and H-Nb_2O_5. (a) A view down the c direction and (b) a view along a direction of T-Nb_2O_5. (c) A view down the b direction and (d) a view along [101] direction of H-Nb_2O_5. Oxygen sites are represented by purple spheres. Polyhedra in different layers are highlighted by different color (i.e., light blue and dark blue). The tetrahedra connecting the corners of the blocks in H-Nb_2O_5 are highlighted by brilliant blue for contrast. The boxes with dashed white lines indicate the unit cells.

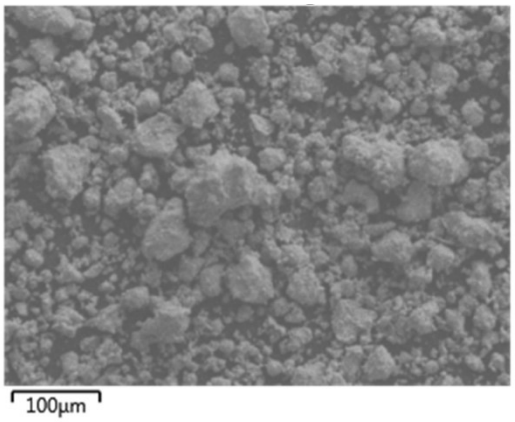

Element	Atomic %
C	45.85
O	37.16
Nb	16.99
Total:	100

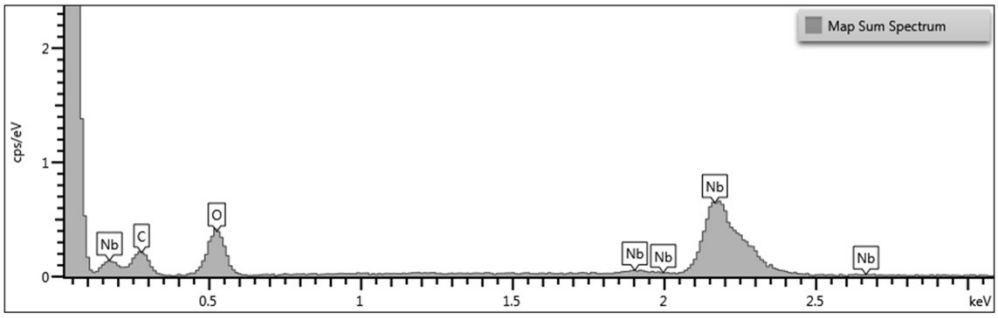

Figure S2. Energy-dispersive X-ray spectroscopy of Nb_2O_5 hydrate. The EDS does not indicate the presence of any other element except for carbon which comes from the carbon tape substrate.

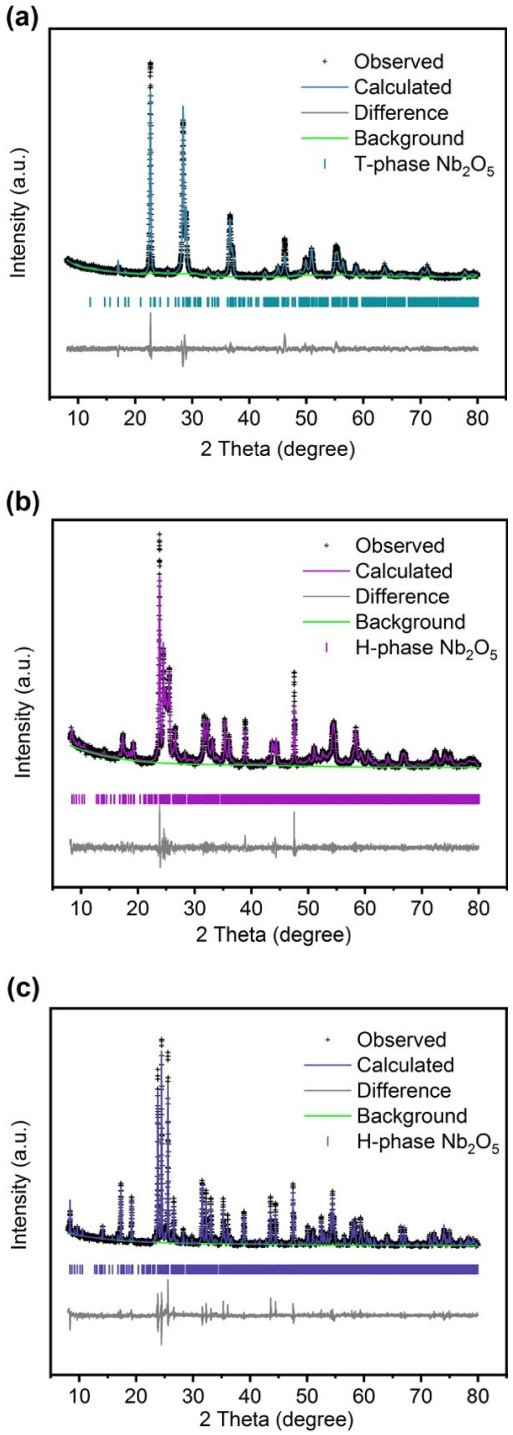

Figure S3. XRD refinement of the Nb_2O_5 hydrate calcined at (a) 700 °C (b) 950 °C, and (c) 1300 °C, respectively. Rietveld refinement was performed for the samples prepared at 700 °C and 1300 °C. Le Bail fitting was performed for 950 °C sample since Rietveld refinement by theoretical model of H-Nb_2O_5 of either P2 or P2/m group could not give good fit, indicating the sample are not long-range ordered.

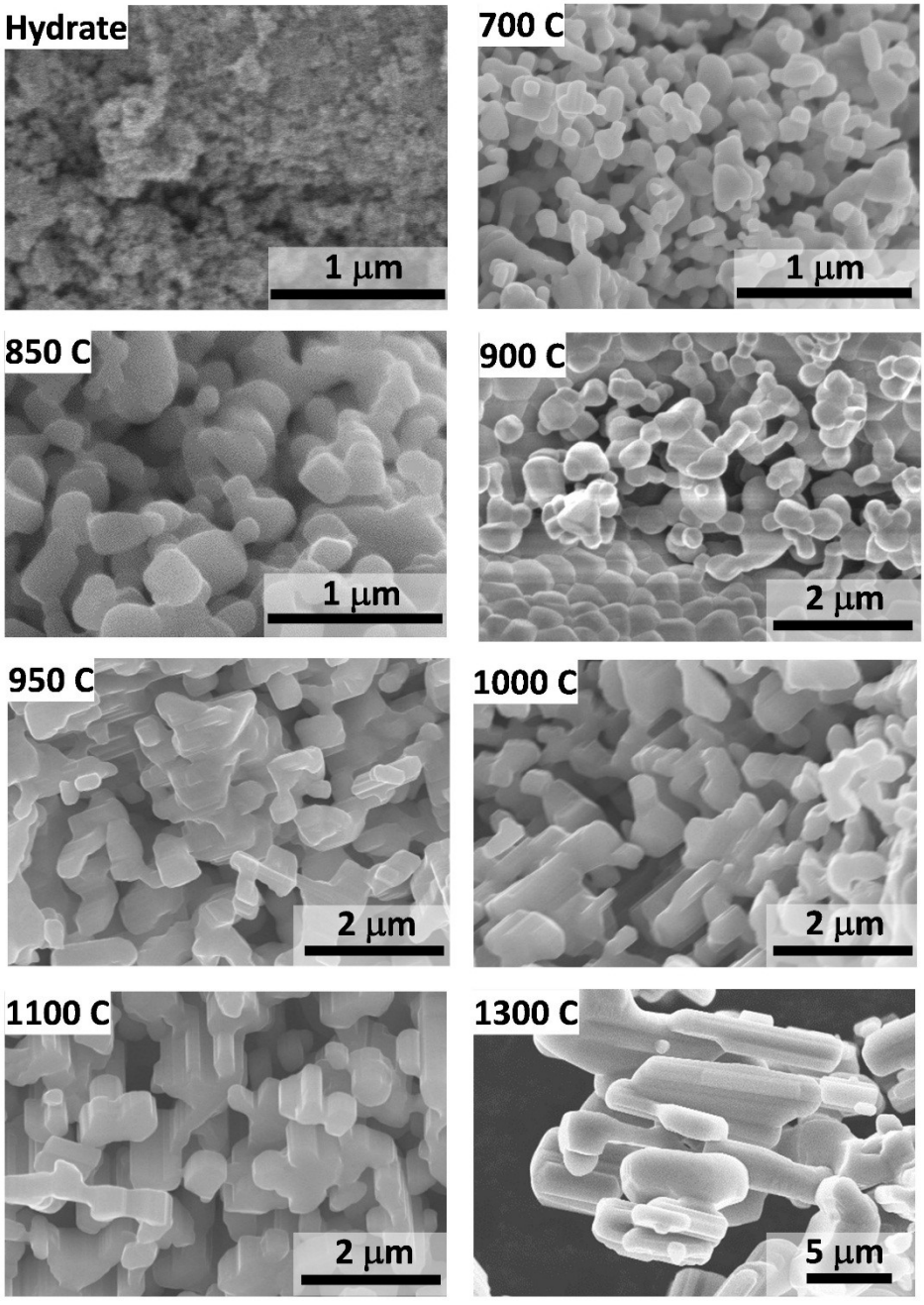

Figure S4. SEM images of the Nb_2O_5 polymorphs obtained by annealing Nb_2O_5 hydrates at different temperatures. Synthesis temperature are denoted.

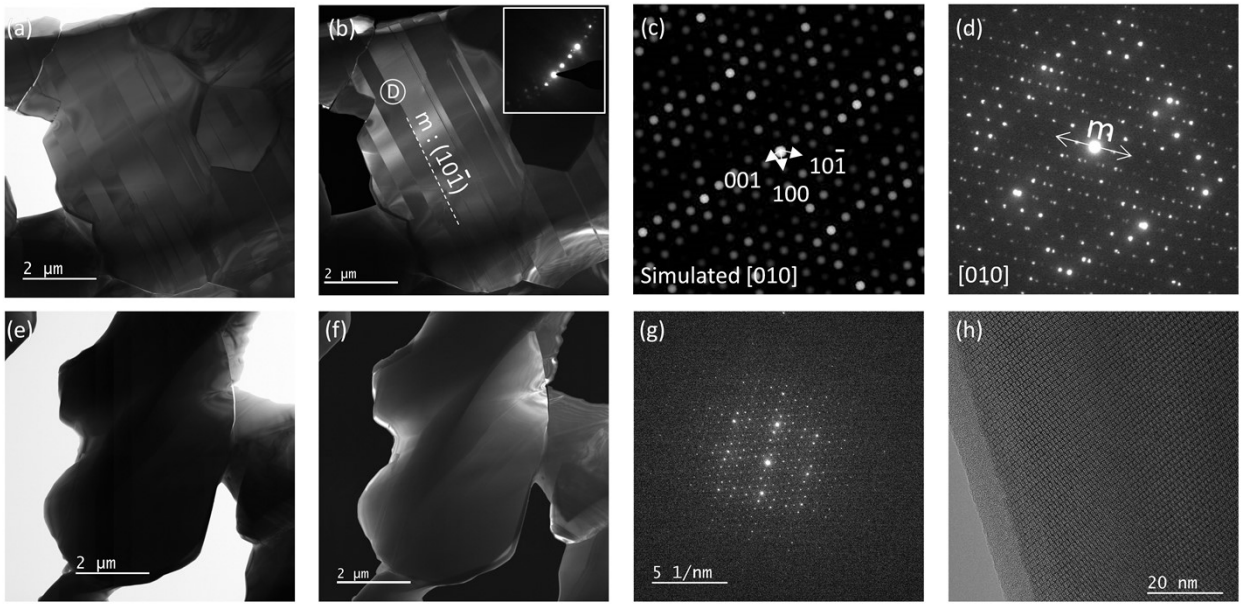

Figure S5. TEM images of Nb_2O_5 prepared at 1300 ^oC; grain with incident electron beam along [010] direction. (a) Bright-field and (b) dark-field TEM images of Nb_2O_5 prepared at 1300 ^oC. Figure a and b here is identical images with Figure 2c in the manuscript but with different magnification. (c) Simulated electron diffraction pattern of H-Nb_2O_5 along [010] direction. (d) Electron diffraction pattern from the crystal imaged in area D in (b) along [010] direction. (e) Bright-field, (f) corresponding dark-field TEM images and (g) SAED pattern of another grain of Nb_2O_5 prepared at 1300 ^oC. (h) The typical high-resolution TEM images of Nb_2O_5 prepared at 1300 ^oC showing the long-range order of the structure.

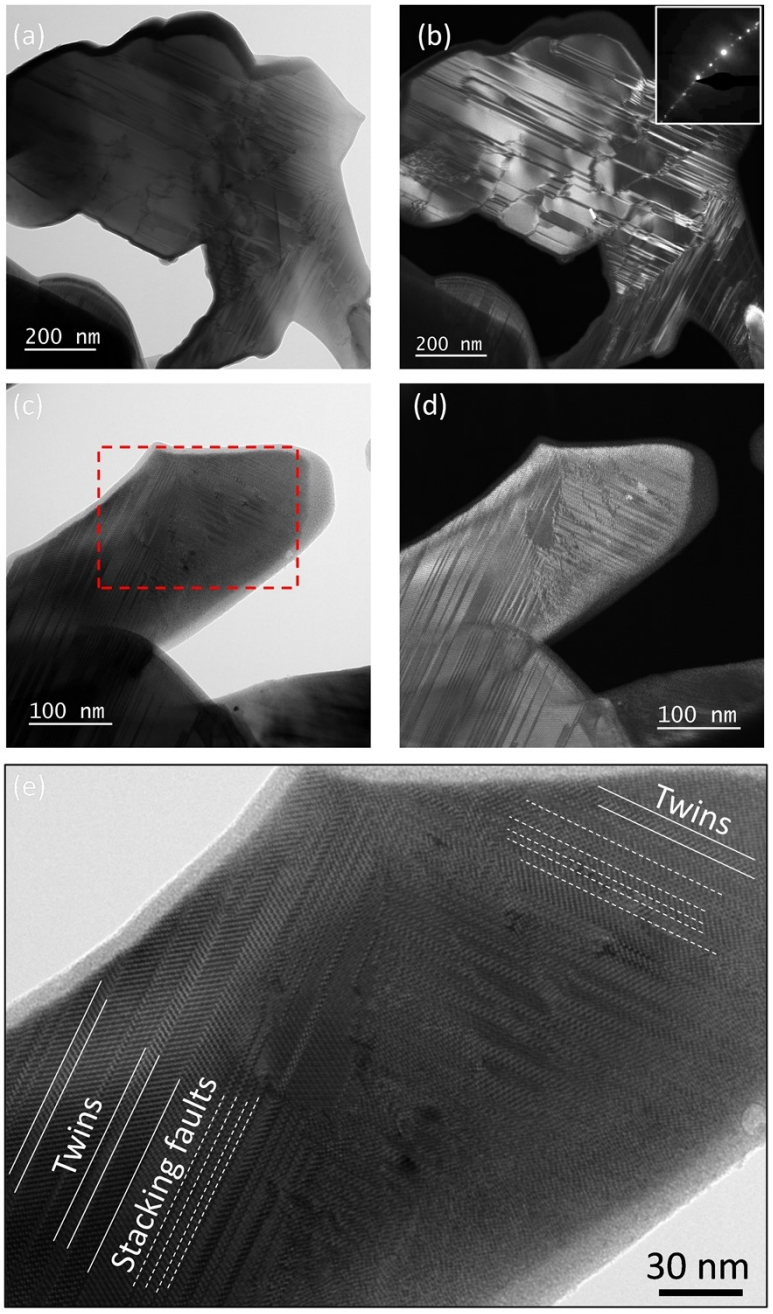

Figure S6. (a, c) Bright-field, (b, d) corresponding dark-field TEM images of Nb_2O_5 prepared at 950 °C captured from [010] direction. (e) High-resolution TEM images of enclosed area in (c). Inset in (b) is the diffraction condition used to form the dark field. Figure 2f is derived from Figure S6b. The abundant stacking faults and sub-twins can be observed by different contrast. Twins and stacking faults were labeled as solid and dash line in (e), respectively. The as-observed thin amorphous layer of the materials is caused by the ion-milling process during TEM sample preparation.

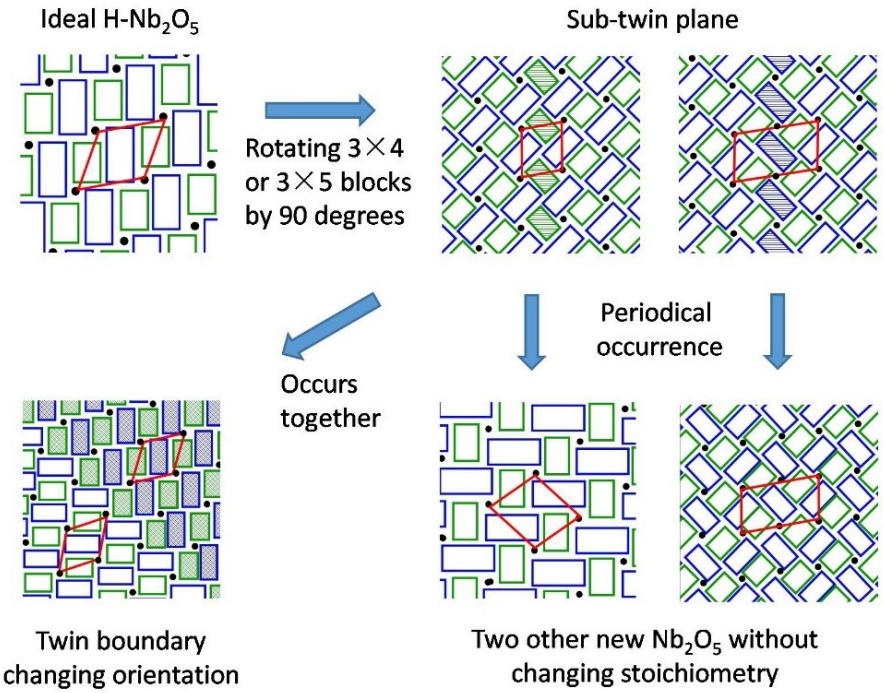

Figure S7. Models showing formation of several micro-domains by sub-twins in Nb_2O_5 prepared at 950 °C. The models are derived from a previous study.[7] The blue and green squares representing 3 × 5 and 3 × 4 building blocks of ideal H-Nb_2O_5. The same kind of defects were observed by quenching H-Nb_2O_5 from melt in previous study[7], while in our work an appropriate annealing temperature could result in H-Nb_2O_5 with these abundant planar defects.

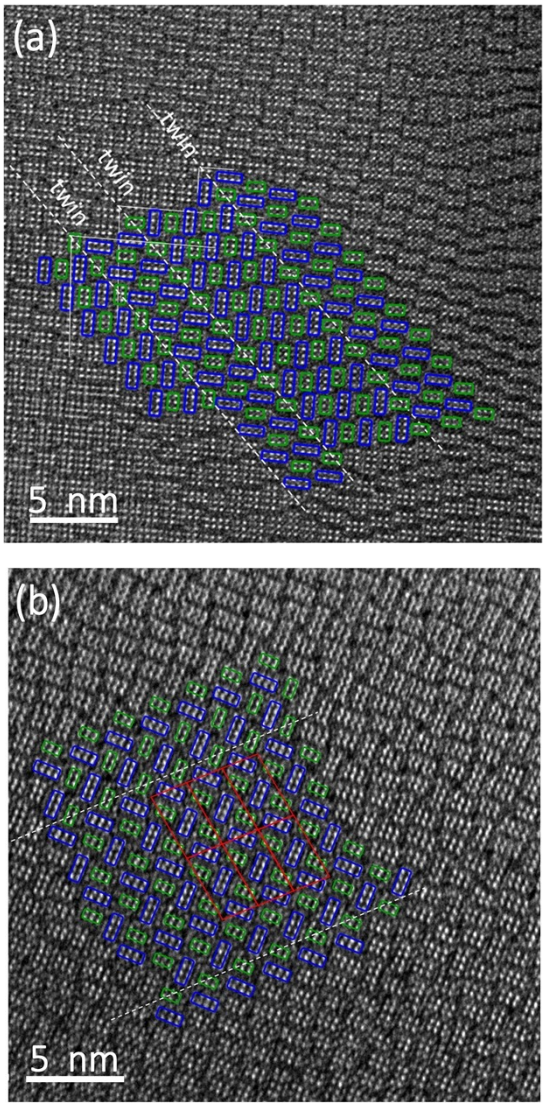

Figure S8. HR-TEM images with models showing formation of several micro-domains by sub-twins in Nb_2O_5 prepared at 950 ^oC. The darker and lighter squares representing 3 × 5 and 3 × 4 building blocks of ideal H-Nb_2O_5. Red rhomboid in (b) represents several unit cells of a new Nb_2O_5 formed by these periodical twins, which denoted as d_2-H-Nb_2O_5 in the following DFT calculation.

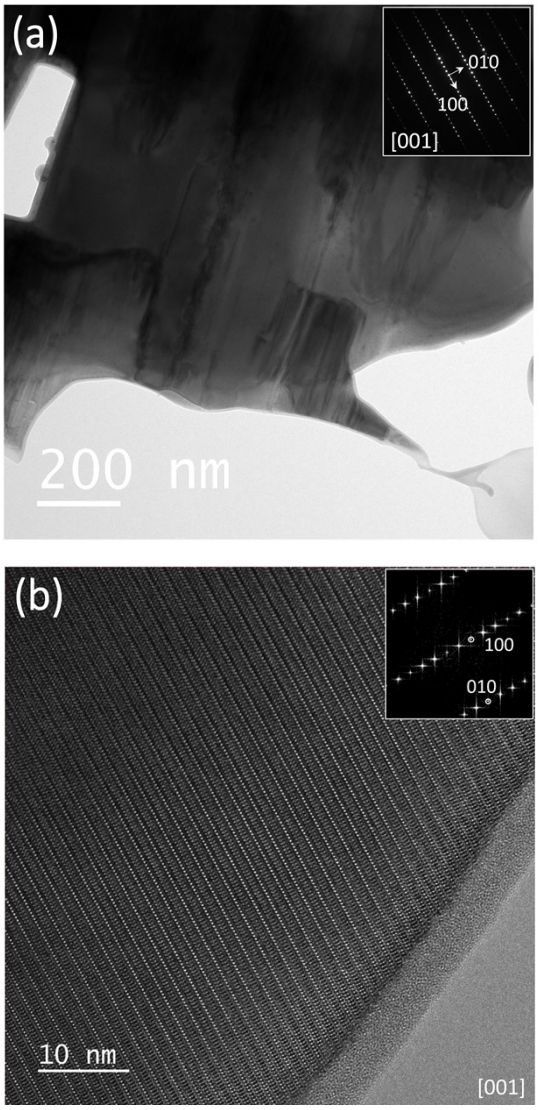

Figure S9. (a) TEM and (b) HR-TEM images of sample calcined at 950 ^{o}C along c axis. Insets in (a) and (b) are the corresponding SAED pattern and Fast Fourier transform (FFT) pattern, respectively. No disorder was observed in ab plane in both short and long-range.

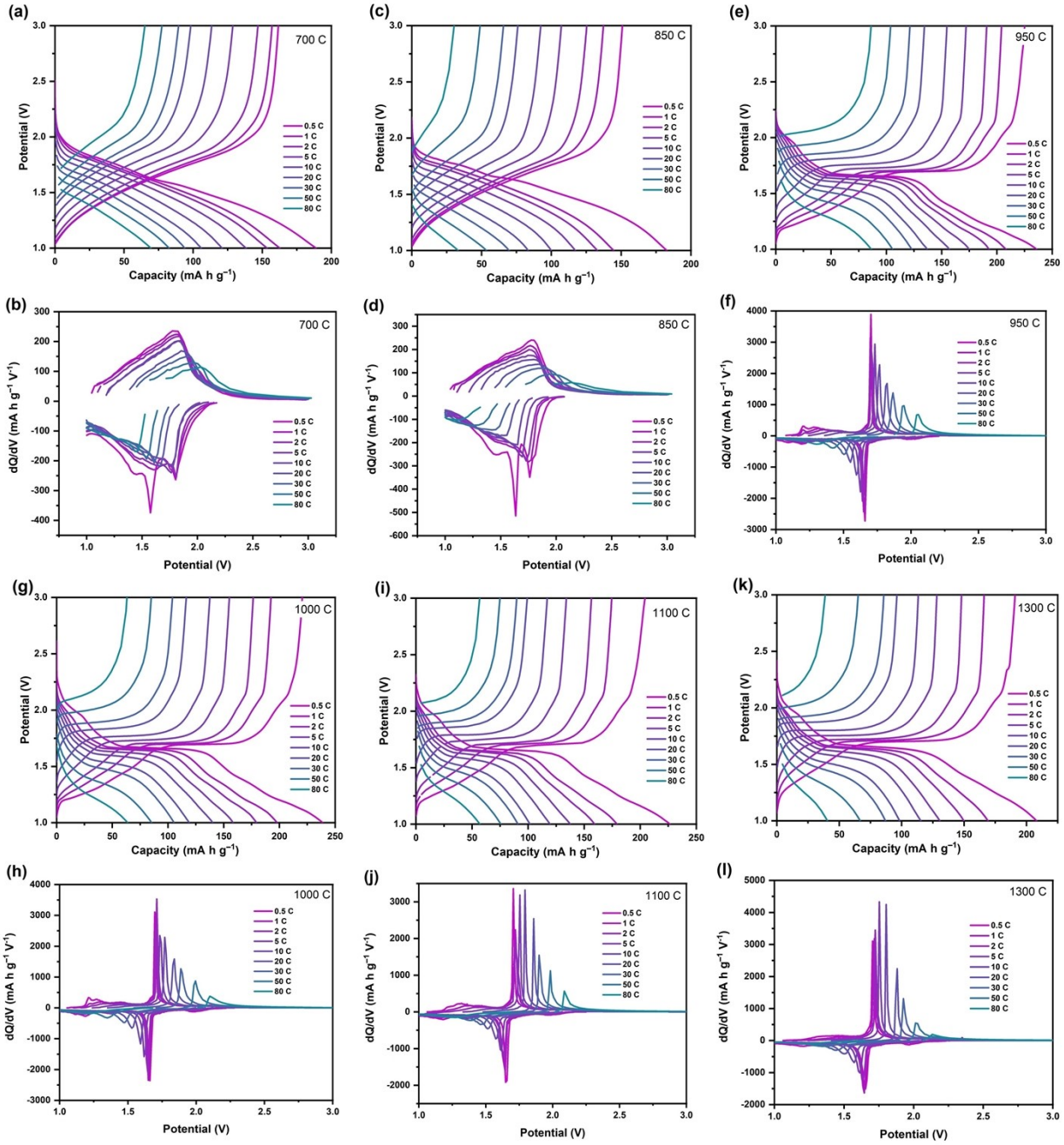

Figure S10. Discharge-charge curves of (a, c) T-Nb_2O_5, (e, g, i) d-H-Nb_2O_5 and (k) H-Nb_2O_5 at various current densities. (b, d, f, h, j, i) The corrsponding dQ/dV plots derived from the discharge/charge curves. The preparation temperature are denoted.

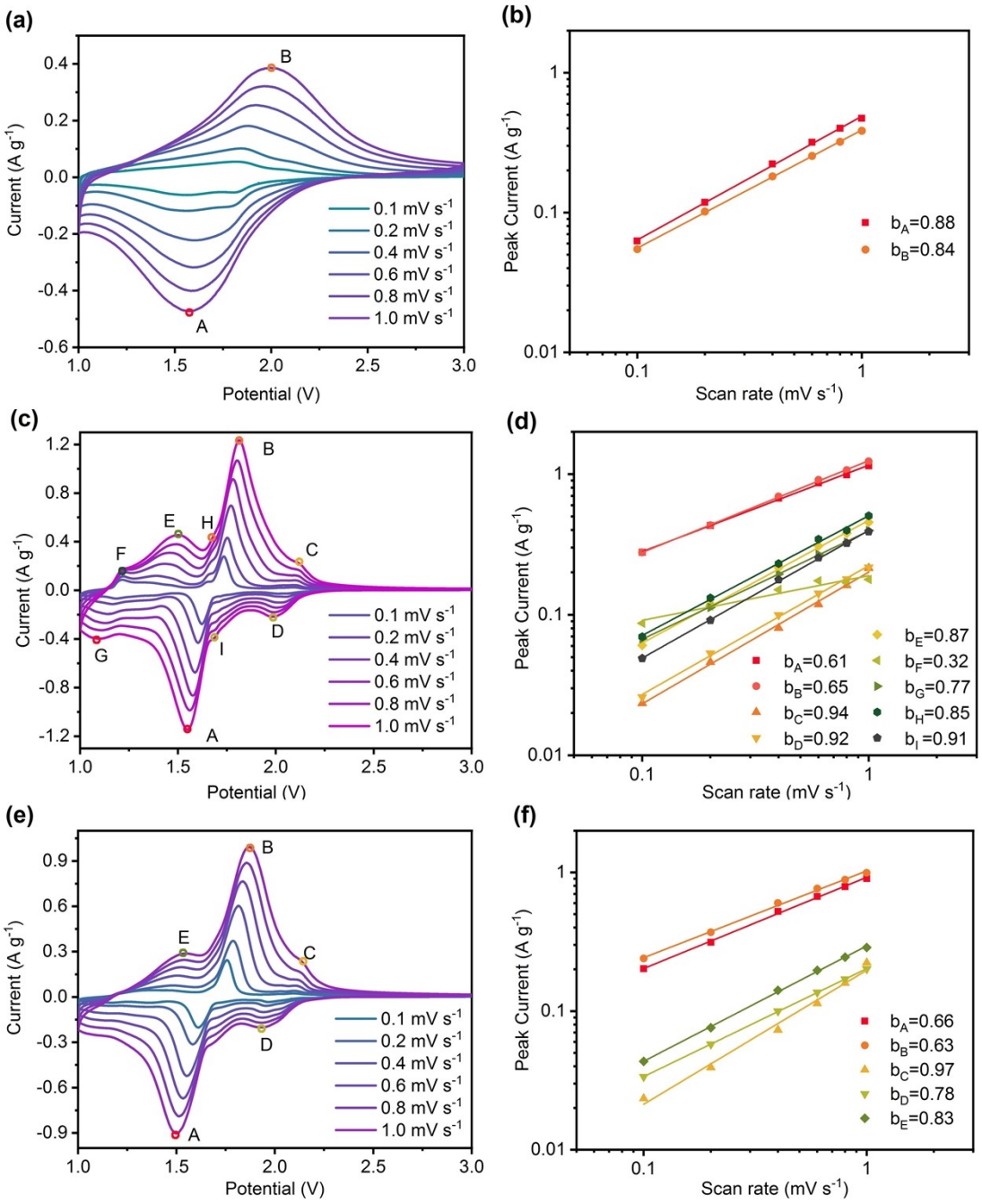

Figure S11. CV curves of (a) T-Nb_2O_5, (c) d-H-Nb_2O_5 and (e) H-Nb_2O_5, at various sweep rates. (b, d, f) their corresponding power law fits for each re-dox peak. b value was calculated for each peak according to $Ip = av^b$, where Ip is the peak current, v the voltage sweep rate, and a and b are fitting parameters.

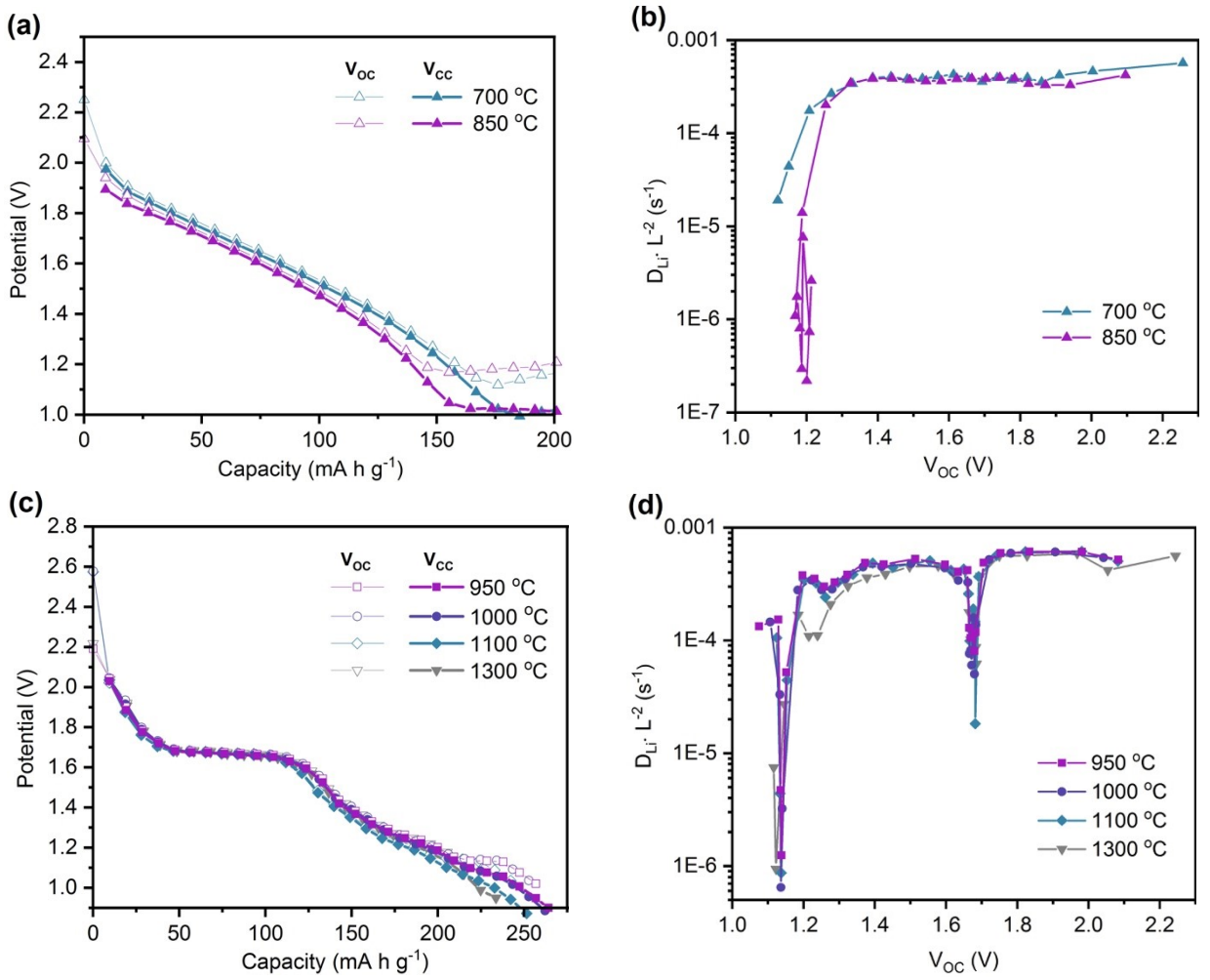

Figure S12. GITT curves for (a) T-Nb_2O_5 and (c) H-Nb_2O_5 with and without defects. (b, d) $D_{Li}L^{-2}$ value, relative Li^+ ions diffusion coefficients of Nb_2O_5, calculated from corresponding GITT curves.

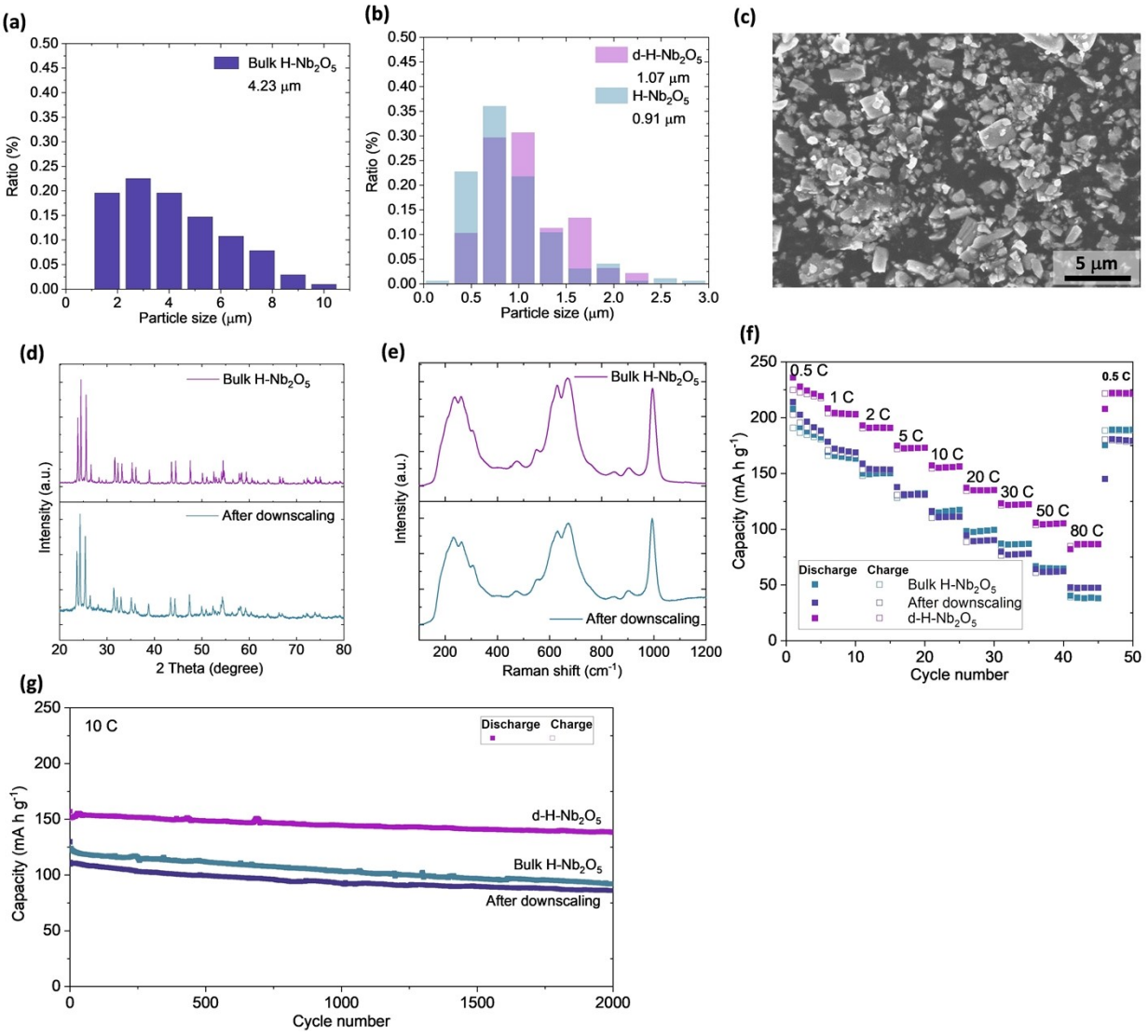

Figure S13. (a) The distribution of particle size of H-Nb_2O_5 prepared at 1300 C. The average size is around 4.23 μm. (b) the distribution of particle size of d-H-Nb_2O_5 and H-Nb_2O_5 after down scaling process by roller milling. A closer particle size was achieved by this process. (c) SEM image of H-Nb_2O_5 after roller milling. The comparison of (d) XRD patterns and (e) Raman spectra of H-Nb_2O_5 before and after down scaling. (f) Rate performance of the Nb_2O_5 samples at various current densities. (g) Cycling performance of different Nb_2O_5 at 10 C.

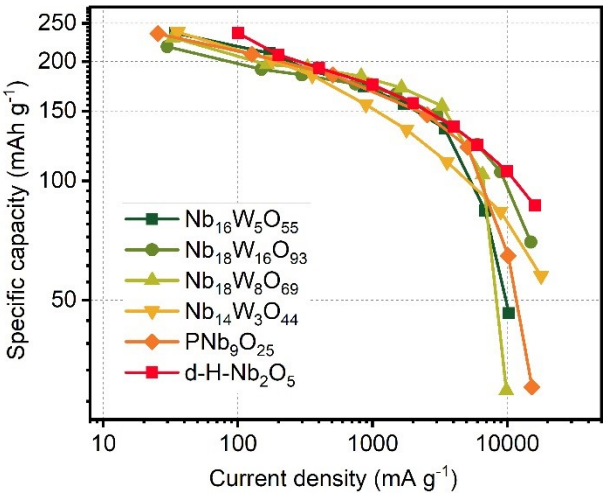

Figure S14. The comparison of specific capacities of d-H-Nb_2O_5 at various current densities with results of recently reported niobium-based oxides. The electrodes in present work were prepared by mixing the active material, carbon black (Super P) and PVDF binder in a weight ratio of 8:1:1. The mass loading was between 1 and 1.5 mg cm^{-2}. The ratio of active materials, carbon and binder in PNb_9O_{25} work is 7.5:1.5:1. The ratio of active materials, carbon and binder (CMC: SBR = 1: 1) in $Nb_{14}W_3O_{44}$ work is 7:2:1. It should be noted that the mass loading of $Nb_{18}W_8O_{69}$ is 2.0 ± 0.2 mg·cm^{-2}. The mass loading of $Nb_{16}W_5O_{55}$ and $Nb_{18}W_{16}O_{93}$ is between 2 and 3 mg cm^{-2} but it was charged with a 1-h constant-voltage step for $Nb_{16}W_5O_{55}$. Unless otherwise noted, the other parameter for the comparison is same.

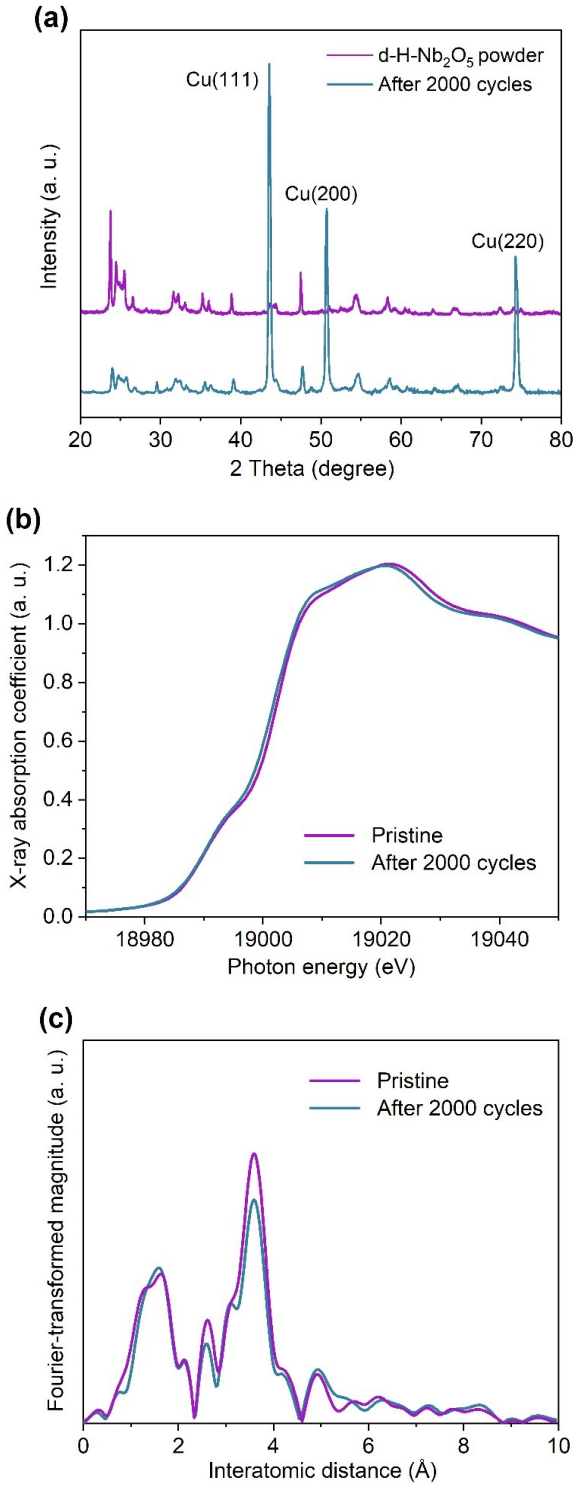

Figure S15. (a) XRD pattern of d-H-Nb_2O_5 electrode after stability test at 10 C for 2,000 cycles; XRD pattern of initial d-H-Nb_2O_5 powder is shown for comparison. Ex-situ (b) XANES spectra and (c) RDF profile of Nb K-edge EXAFS spectra of d-H-Nb_2O_5 electrode before and after stability test at 10 C for 2000 cycles.

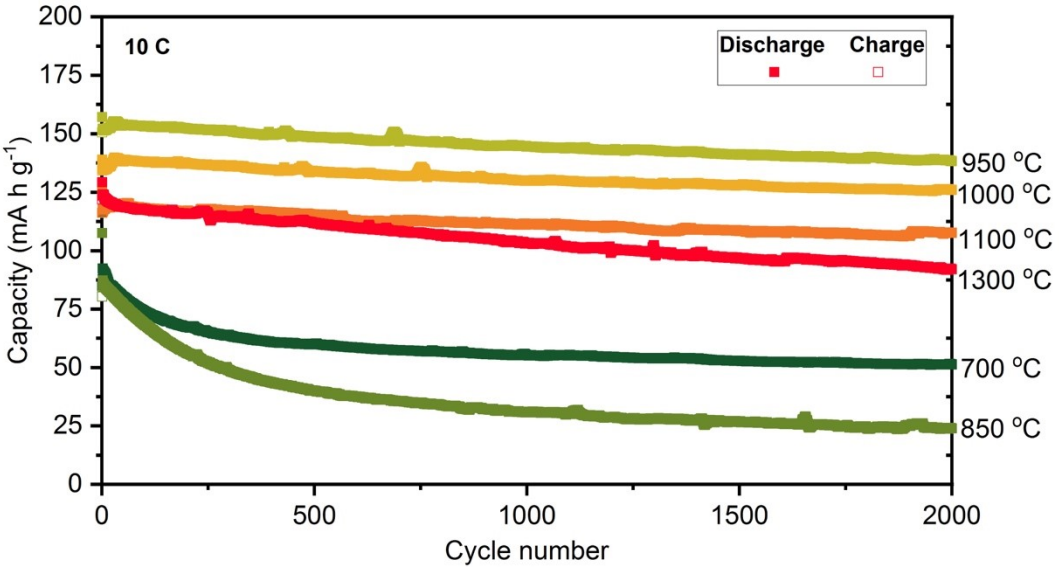

Figure S16. Cycling performance of Nb_2O_5 prepared at different temperatures at potential window from 3.0 to 1.0 V versus Li^+/Li at 10 C. T-Nb_2O_5 shows a rapid degradation at 10 C regardless of temperature while H-Nb_2O_5 especially defective derivate (950 -1100 °C) show a good preservation of the capacity.

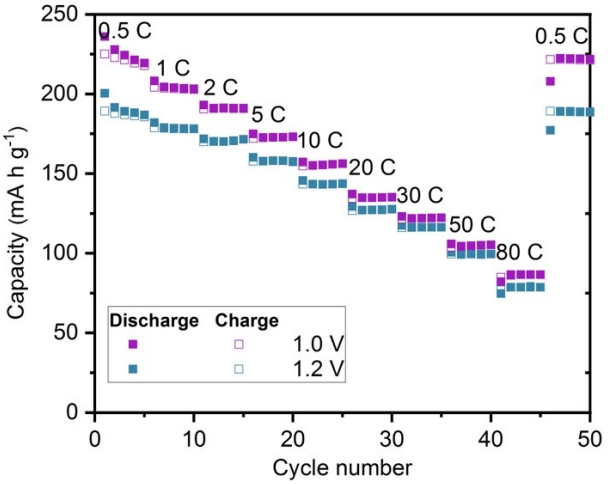

Figure S17. Effect of potential window from 3.0 to 1.2/1.0 V versus Li^+/Li on rate performance of d-H-Nb_2O_5 (950 ^oC).

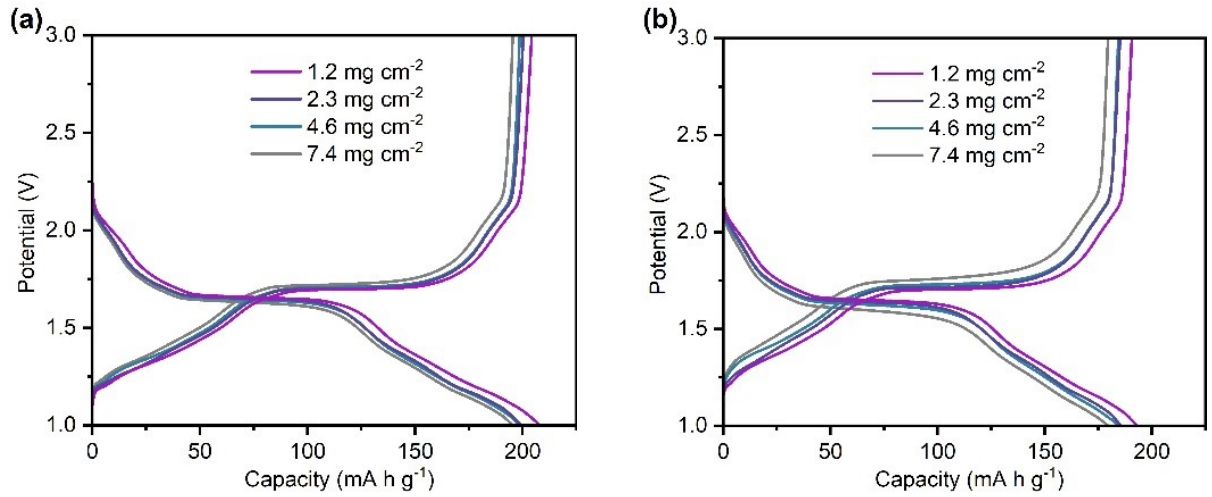

Figure S18. The charge/discharge curve of d-H-Nb_2O_5 at the different mass loading at (a) 1 C and (b) 2 C.

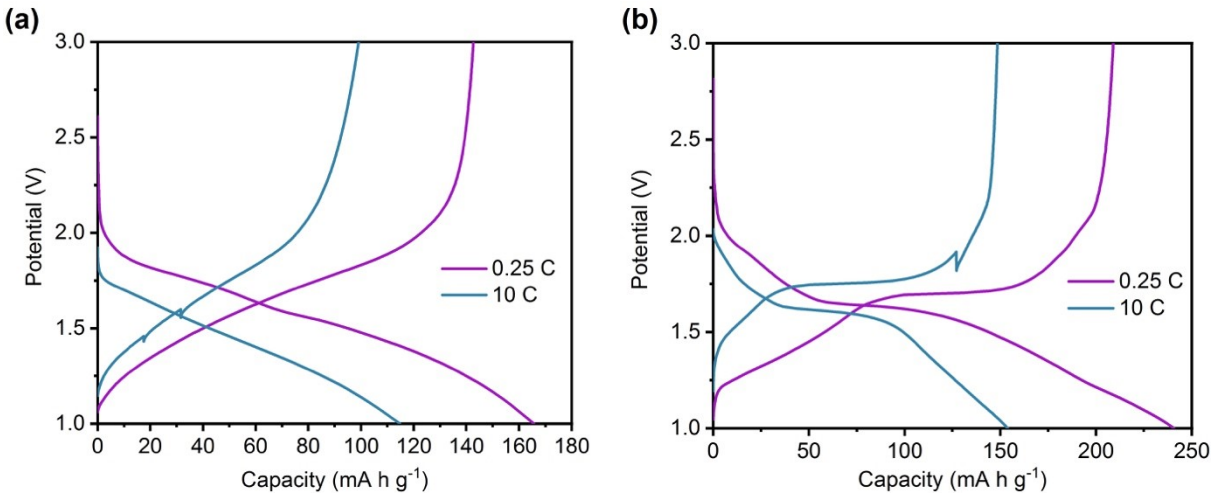

Figure S19. Charge and discharge curves of pouch cell of (a) T-Nb_2O_5 and (b) d-H-Nb_2O_5 measured for operando XAS analysis.

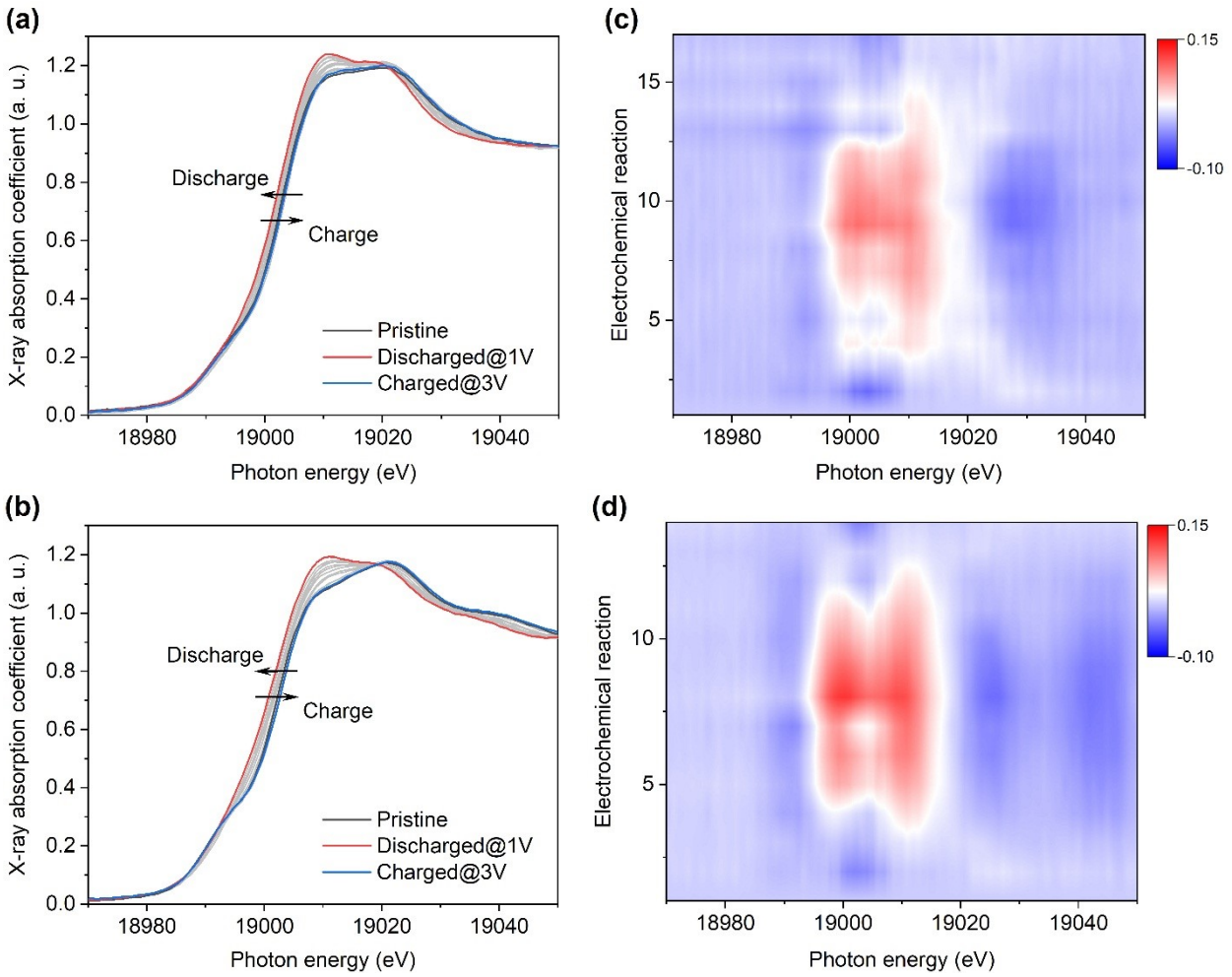

Figure S20. Operando Nb K-edge X-ray absorption near edge structure (XANES) profiles for the electrode of (a) T-Nb_2O_5 and (b) d-H-Nb_2O_5 at 10 C during cycling. 2D contour plot of operando XANES variation for (c) T-Nb_2O_5 and (d) d-H-Nb_2O_5 during cycling.

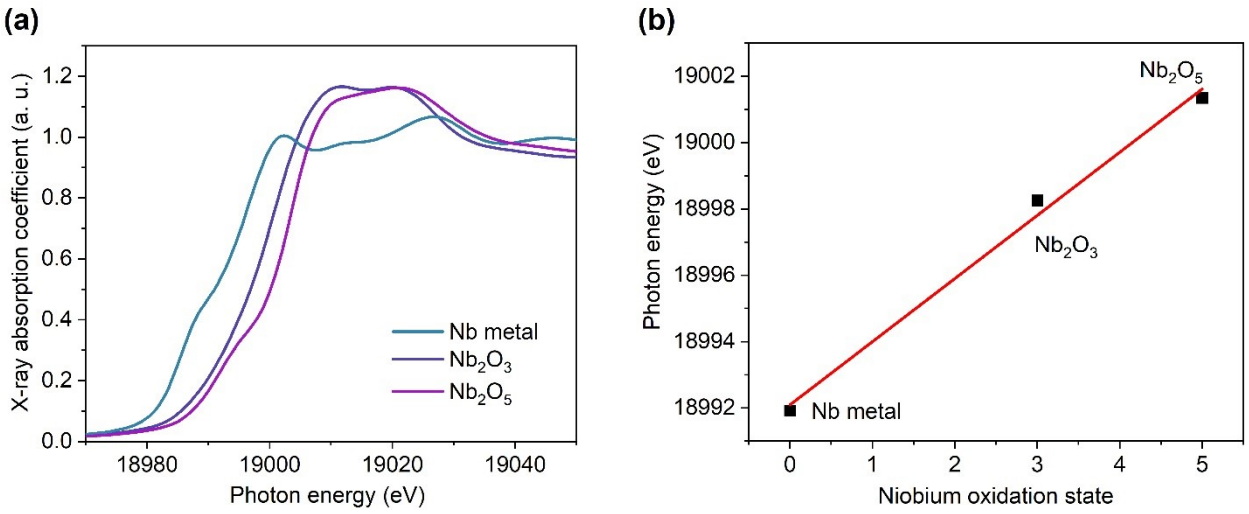

Figure S21. Chemical valence calibration. (a) Nb-edge XANES spectra of reference standard materials and (b) their valance state relationship with edge adsorption position. All the edge energy for calibration were taken at the position of half of the edge step height.

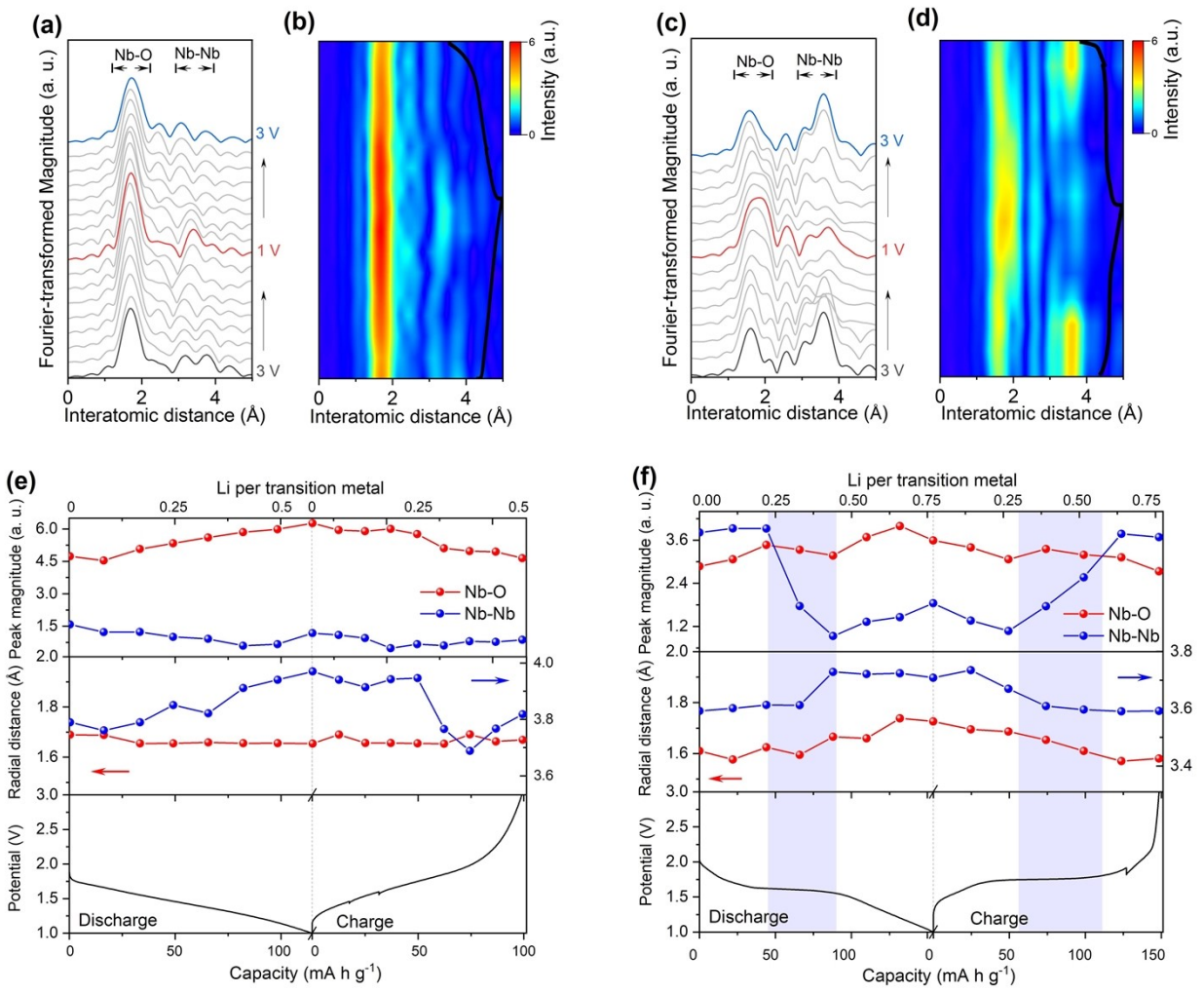

Figure S22. Radial distribution function (RDF) of Nb K-edges operando EXAFS spectra and their corresponding 2D contour plot for the electrode of (a, b) T-Nb_2O_5 and (c, d) d-H-Nb_2O_5 at 10 C. The electrochemical discharge/charge profile (black curve) of operando cell was overlaid in the right side of contour plot. (e, f) peak magnitudes and radial distance derived from RDF (a, c) as functions of electrochemical reaction.

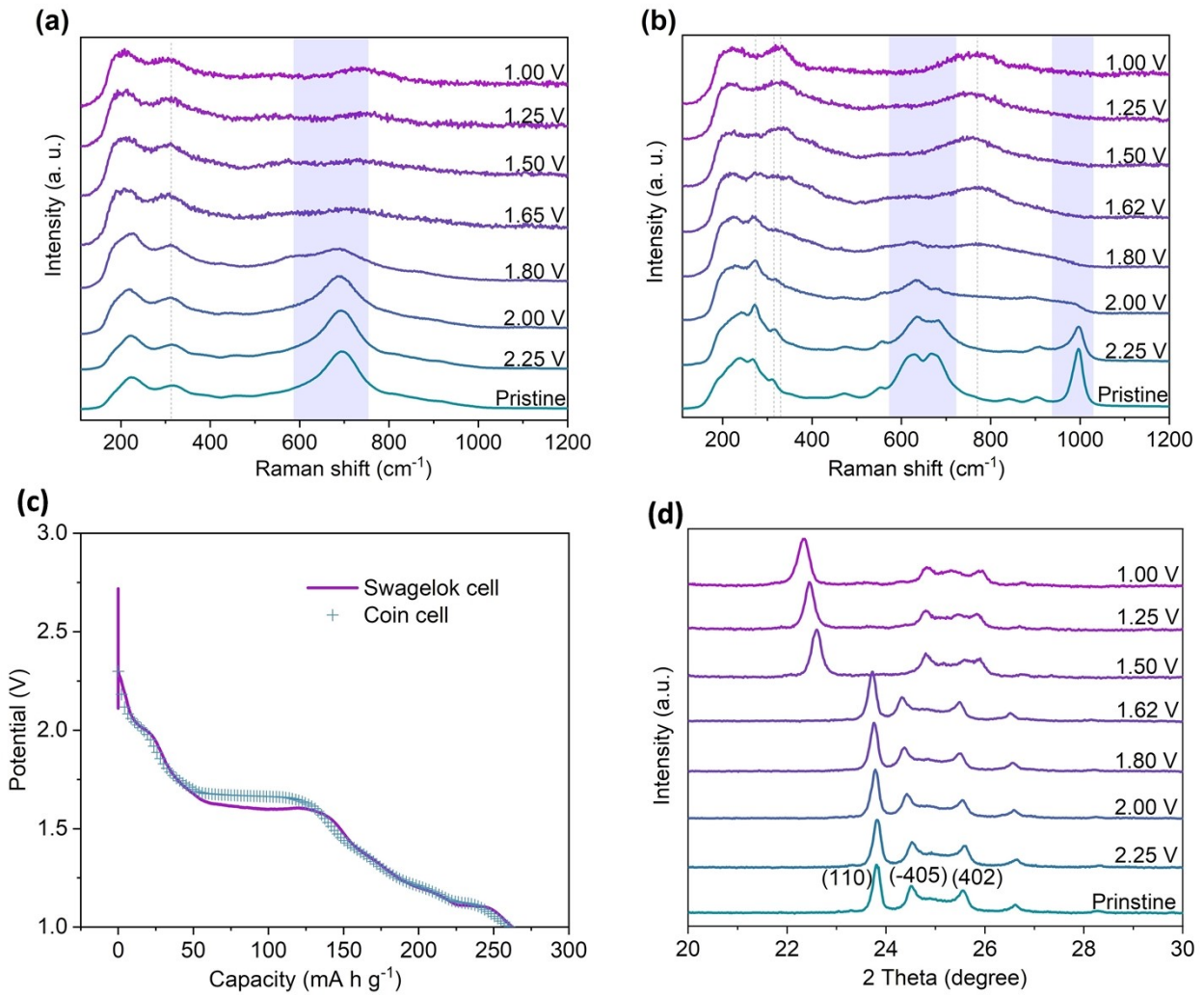

Figure S23. (a) Ex-situ Raman spectra of (a) T-Nb_2O_5 and (b) d-H-Nb_2O_5 samples upon lithiation. (c) The comparison of discharging curve of d-H-Nb_2O_5 by using conventional coin cell at 0.05 C, and Swagelok cell at 0.0026 C. d-H-Nb_2O_5 was discharged in Swagelok cell without adding carbon and binder in order to for Ex-situ (Raman and XRD) study. A slight polarization at two phase region was observed for the Swagelok cell. (d) Ex-situ XRD pattern for lithiated d-H-Nb_2O_5. Before two-phase region (1.62 V for Swagelok cell), a solid solution reaction was observed for d-H-Nb_2O_5.

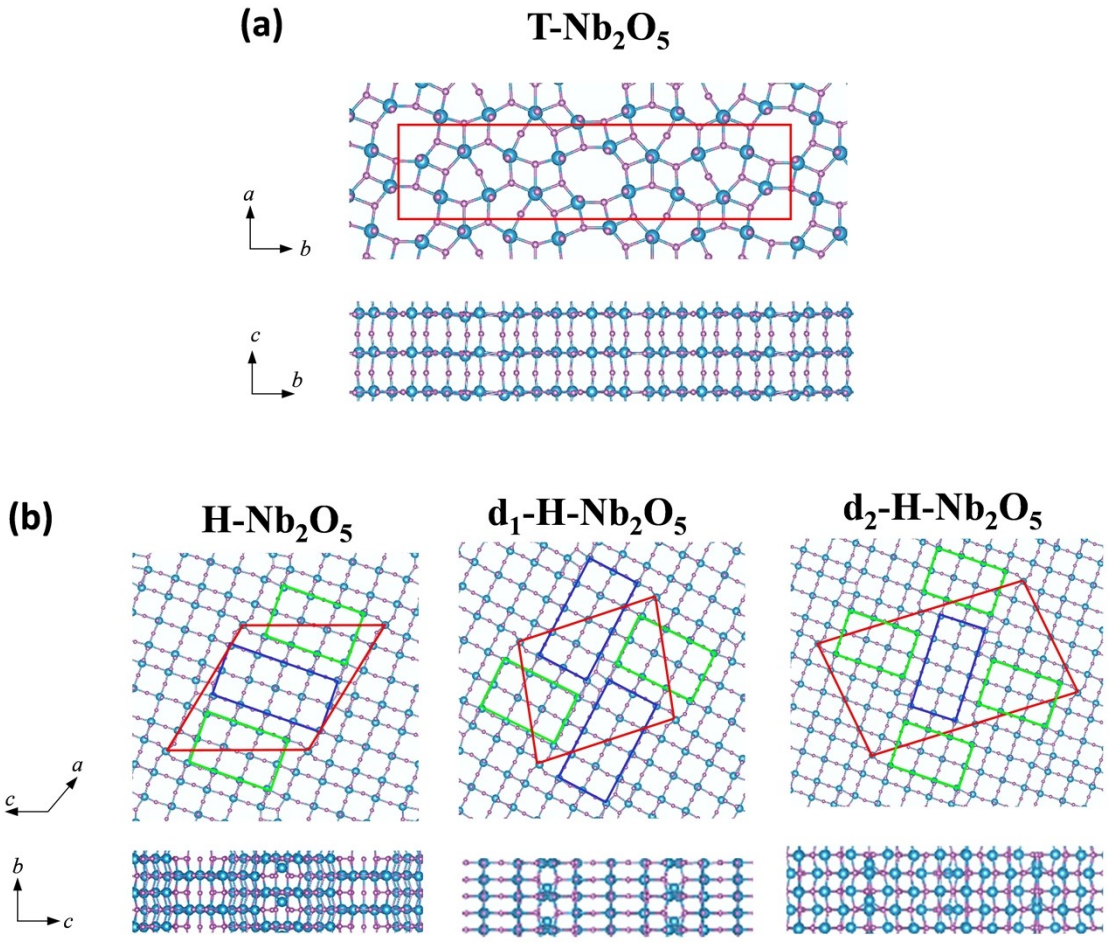

Figure S24. Top and side views of the (a) T-Nb_2O_5 and (b) H-Nb_2O_5, d_1-H-Nb_2O_5 and d_2-H-Nb_2O_5. The boxes with red lines indicate unit cells; green and blue rectangles indicate 3×4 and 3×5 blocks, observed in TEM (Figure 2e and 2h); Nb, O and Li are represented with blue, purple and green balls, respectively.

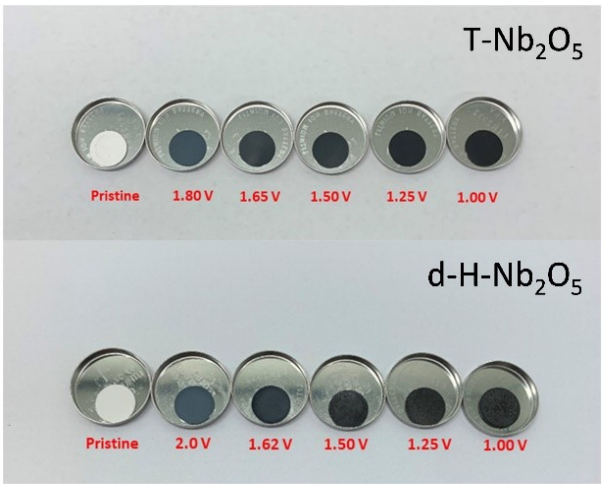

Figure S25. The change in color of the lithiated Nb_2O_5 pellets suggests increased electronic conductivity upon lithiation.

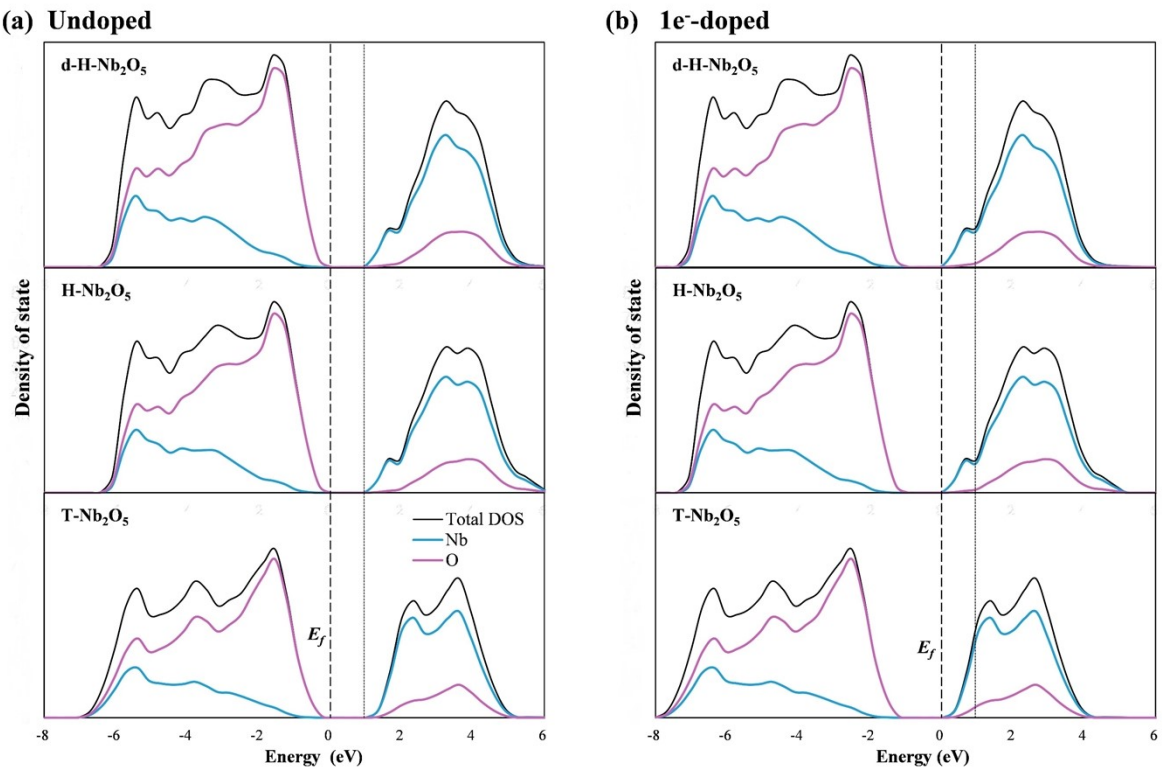

Figure S26. Density of states (DOS) for (a) pristine and (b) electron-doped Nb_2O_5. The left dashed line in every figure represents the Fermi energy (E_f).

Table S1. BET surface area for Nb_2O_5 obtained by anealling hydrate at different temperatures.

Temperature	700 °C (T-Nb_2O_5)	850 °C (T-Nb_2O_5)	950 °C (d-H-Nb_2O_5)	1000 °C (d-H-Nb_2O_5)	1100 °C (d-H-Nb_2O_5)	1300 °C (Bulk H-Nb_2O_5)	1300 °C (H-Nb_2O_5 after downscaling)
BET surface area ($m^2\ g^{-1}$)	8.17	1.96	1.03	0.93	0.89	0.35	3.87

Reference

1. Momma, K.; Izumi, F., *J. Appl. Crystallogr.*, 2011, **44**, 1272-1276.
2. Stadelmann, P. A., *Ultramicroscopy*, 1987, **21**, 131-145.
3. Sale, M.; Avdeev, M., *J. Appl. Crystallogr.*, 2012, **45**, 1054-1056.
4. Griffith, K. J., University of Cambridge, 2018.
5. Weppner, W.; Huggins, R. A., *J. Electrochem. Soc.*, 1977, **124**, 1569-1578.
6. Rohatgi, A., WebPlotDigitizer. *https://automeris.io/WebPlotDigitizer* 2020.
7. Iijima, S., *Acta Crystallogr., Sect. A*, 1973, **29**, 18-24.